Hindawi
Mathematical Problems in Engineering
Volume 2018, Article ID 6386513, 12 pages
https://doi.org/10.1155/2018/6386513

Research Article

The Fractional Order PID Method with a Fault Tolerant Module for Road Feeling Control of Steer-by-Wire System

Fei-xiang Xu, Xin-hui Liu, Wei Chen, Chen Zhou, and Bing-wei Cao

School of Mechanical and Aerospace Engineering, Jilin University, Changchun 130022, China

Correspondence should be addressed to Wei Chen; chenwei_1979@jlu.edu.cn

Received 20 August 2018; Accepted 5 November 2018; Published 19 November 2018

Academic Editor: Saeed Eftekhar Azam

To improve the road feeling of the steer-by-wire (SBW) system, a fractional order PID (proportion-integral-derivative) method with a fault tolerant module is proposed in this paper. Firstly, the overall road feeling control strategy of the SBW system is introduced, and then the mathematical model of road feeling control is established. Secondly, a fractional order PID (FOPID) controller is designed to control torque of the road feeling motor. Furthermore, genetic algorithm (GA) is applied to tune the FOPID controller's parameters. Thirdly, a fault tolerant module aiming at potential failures of the motor's torque sensor is studied to improve the reliability of the system. Kalman Filter (KF) algorithm is utilized in the fault tolerant module so as to detect failures of the motor's torque sensor, and then fault tolerant module reconfigures the motor's torque estimated by KF as a substitute when the torque sensor fails. Finally, simulations based on MATLAB are performed with the proposed control strategy to identify its performance, and the results demonstrate that the proposed control method is feasible and accurate.

1. Introduction

The SBW system is playing an important role in the development of modern vehicles [1, 2], which breaks the concept of traditional steering system and replaces the mechanical joint between the steering wheel and front wheels [3]. The SBW system not only simplifies the design of cab, but also enhances the vehicle stability and driving force [4]. Drivers will not feel the road condition directly without the mechanical connection from steering wheel to the road in the SBW system [5]. Hence, it is urgent to study the control strategy to improve the road feeling of the SBW system. The road feeling control is to feed back the road condition to the driver, which controls the reaction torque that the steering wheel actuator generates [6].

Recently, some scholars have developed PID controller for the road feeling control of the SBW system [7, 8]. Compared with the PID controller, the FOPID controller adds two adjustable parameters (integral order and derivative order), which provides a larger tuning space for better control performance and robustness [9, 10]. In some practical applications, it is verified that the FOPID controller has better disturbance rejection ability and less sensitivity to the parameter variations of the control system than the traditional PID controller [11]. As a result, the common PID controller is gradually replaced by the FOPID controller with the support of the researchers [12–14]. Therefore, the FOPID controller is adopted to control the road feeling of the SBW system in this paper.

The additional varying orders of integration and differentiation of the FOPID controller are accompanied with the increase of the difficulty of parameters optimization [11]. GA is widely regarded as a global optimization method, which can only depend on the fitness function to search the best parameters with constraints, targets, and dynamic components [15, 16]. With its optimization characteristics, GA has been applied to the parameter optimization of the FOPID controller for many times [17–19]. In this way, GA is used to tune the FOPID controller's five parameters including proportional constant, integral constant, derivative constant, integral order, and derivative order.

Most of the literatures about the FOPID controller and PID controller mentioned above only take into account the case without sensor faults in the control process. The torque sensor is so essential that it is used to measure the feedback signal of the road feeling control system. However,

the faults of the torque sensor could occur in the process of road felling control, which can cause a critical effect on the road feeling control [20]. Consequently, fault tolerant control (FTC) becomes the key issue to ensure the reliability of the control system. Fault detection and diagnosis (FDD) module is essential in FTC problem and it is expected to be very important for general SBW technique [21]. Once the sensor faults occur, the FDD method can detect, diagnose, and remove the faults, thus ensuring the normal working of the control system. The most convenient FDD method for sensors is hardware redundancy, where multisensors are deployed to measure the same physical parameter and faults are detected by comparing all sensor's measurements [21]. For the hardware redundancy method, on the one hand, it is difficult to install multiple redundant sensors on the vehicle; on the other hand, it also increases the development cost. To make up the shortcomings of the hardware redundancy method, the model-based techniques have been widely used in the FDD [22–24], which provides a great fault detection effect and robustness against external disturbances and model uncertainties [25].

The primary principle of the model-based FDD method is to design an observer to evaluate a residual signal which is the difference between the measured signal and the observer output [26]. The model-based FDD method can detect and diagnose sensor faults effectively without redundant hardware. The well-known KF observer is one of the model-based FDD methods, which shows outstanding performance in dealing with the fault tolerant problem, and it has been widely applied to detect and diagnose the sensor faults [27–30]. Zhang Han et al. [5] put forward a fault tolerant module for two-way H infinity controller of the SBW system. KF is used as the FDD method to detect and diagnose front wheel sensor's faults. The simulations and experiments were conducted to verify the proposed FTC strategy based on KF. Xiahou K. S et al. [31] presented a KF-based FTC strategy under voltage and current sensor faults. The sensor faults were detected and isolated based on the residuals calculated from observations measured by sensors and estimations provided by KF. The simulation and experimental studies validated the proposed FTC strategy. Liu Yuan et al. [32] designed a FTC method for aeroengine, where the sensor faults can be diagnosed by KF accurately. The semiphysical simulation indicated that the fault tolerant controller could ensure that the aeroengine controller worked safely and reliably in the event of sensor faults.

Inspired by the previous studies, KF is used to detect and diagnose the torque sensor's faults of road feeling motor in this paper. KF evaluates a residual signal between the measured signal and the observer output. When the value of residual signal is greater than the defined threshold, it indicates that the torque sensor faults occur and the observer output is reconfigured as the reference value of the fault tolerant module. On the contrary, the FOPID controller works normally through obtaining the feedback torque measured by the torque sensor.

In this paper, we aim to improve the driver's road feeling of the SBW system with the FOPID controller tune by GA and KF-based fault tolerant module. The rest of this paper is organized as follows: Section 2 briefly introduces the overall road feeling control strategy; Section 3 studies the design of the FOPID controller; Section 4 focuses on the FTC strategy based on KF; Section 5 describes the simulation results; and the final section is the conclusions.

2. The Overall Road Feeling Control Strategy of the SBW System

2.1. The Structure of the SBW System. The function of SBW system can mainly be divided into two parts: vehicle steering control and road feeling control. The overall structure of the SBW system is shown in Figure 1.

Firstly, the controller receives the angle sensor signal of the steering wheel. Secondly, the controller outputs the currents to the electromagnetic valves. Thirdly, the hydraulic cylinders are pushed by pressure energy from the electromagnetic valves. Finally, the steering of the vehicle is realized. Meanwhile, the pressure sensors installed in the hydraulic cylinders send the steering resistance signal to the controller, and then the controller sends out the control signal to the road feeling motor based on the comparison between the ideal steering resistance torque and the actual torque of the steering wheel detected by the torque sensor. Then the reducing mechanism transfers the torque to the steering wheel. In this way, the road feeling can be obtained by the drivers.

The road feeling control is discussed in this paper, and the vehicle steering control will be studied in the next step.

2.2. The Overall Road Feeling Control Strategy. The closed-loop control method is applied in the road feeling control and the overall road feeling control strategy is shown in Figure 2. The ideal steering resistance torque is calculated by the vehicle speed V and the maximum pressure difference $P_{\max}$ between left cavity and right cavity of four steering cylinders. The concrete formula of the ideal steering resistance torque will be drawn based on experiments conducted on the prototype vehicle in the future. The FOPID controller sends out the control signal to the road feeling motor according to the difference between the ideal steering resistance torque and the torque measured by the torque sensor. The torque sensor is so essential that it is used to measure the feedback signal of the road feeling control system.

The fault tolerant module is used to avoid the bad effect caused by the torque sensor faults of the road feeing control system. KF observer is used to observe the torque output of the road feeling motor and evaluate a residual signal between the measured value and the observer output signal. When the residual signal is greater than the defined threshold, it indicates that the torque sensor faults occur and the value measured by the torque sensor is replaced by the observer output. When the value of the residual signal is smaller than the defined threshold, the FOPID controller works normally through obtaining the feedback torque detected by the torque sensor.

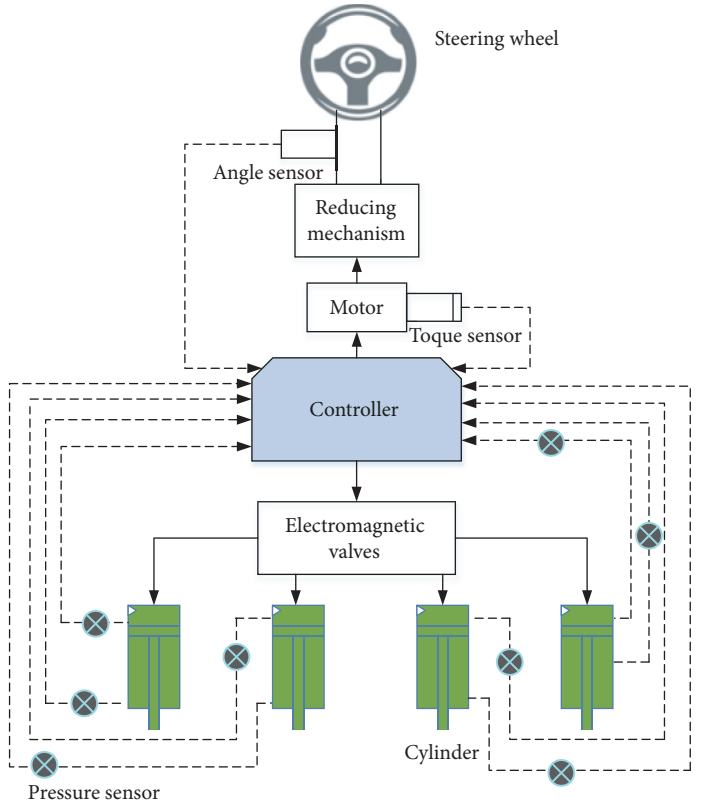

Figure 1: The structure of the SBW system.

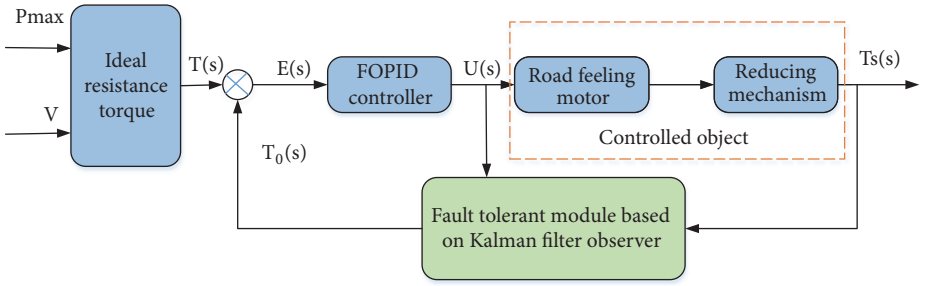

Figure 2: The overall road feeling control strategy. ($T(s)$: the ideal steering resistance torque; $E(s)$: difference between the ideal steering resistance torque and actual steering resistance torque; $U(s)$: the output voltage of the FOPID controller; $T_s(s)$: the output torque of the road feeling motor; $T_0(s)$: the torque reconfigured by the fault tolerant module.)

2.3. System Modelling. The control system modelling is mainly to establish the mathematical model of the road feeling motor, whose moment equilibrium equation is expressed as follows.

$$T_m = J_m \frac{d^2\theta_m}{dt^2} + B_m \frac{d\theta_m}{dt} + K_m \frac{\theta_m / g_m - \theta_{sw}}{g_m} \quad (1)$$

where T_m denotes the output torque of the road feeling motor; J_m represents the moment of inertia of the road feeling motor; B_m stands for the damping coefficient of the road feeling motor; K_m is the torsional stiffness of the road feeling motor; g_m represents the reduction ratio of the reducing mechanism; θ_m is the angle of the road feeling motor; θ_{sw} denotes the steering wheel angle.

The last subformula in formula (1) occupies a small proportion in the whole equation, which can be ignored here [33].

$$T_m = J_m \frac{d^2\theta_m}{dt^2} + B_m \frac{d\theta_m}{dt} \quad (2)$$

The electromagnetic torque and the current of the road feeling motor can be expressed as follows.

$$T_m = K_t I \quad (3)$$

where K_t denotes the torque coefficient of the road feeling motor; I represents the armature current of the road feeling motor.

The electromotive force balance equation of the road feeling motor is shown below.

$$U = L\frac{dI}{dt} + RI + K_e\frac{d\theta_m}{dt} \tag{4}$$

where U denotes the armature voltage of the road feeling motor; L represents the armature inductance of the road feeling motor; R represents the armature resistance of the road feeling motor; K_e is the back electromotive force coefficient of the road feeling motor.

The Laplace transform is carried out for (2)-(4) mentioned above, and the transfer function from torque of the road feeling motor to the output voltage of the FOPID controller can be shown as follows.

$$\begin{aligned} G(s) &= \frac{T_s(s)}{U(s)} = g_m\frac{T_m(s)}{U(s)} \\ &= \frac{g_m K_t J_m s + g_m K_t B_m}{J_m L s^2 + (B_m L + J_m R)s + B_m R + K_t K_e} \end{aligned} \tag{5}$$

The actual parameters of the SBW system in this paper are shown in Table 1.

3. The FOPID Controller Design

3.1. The FOPID Controller. Compared with the conventional PID controller, the FOPID controller adds the integral and differential orders, which makes control system fine tracking accuracy, abundant dynamics, and high robustness [34]. Before describing the design of the FOPID controller, the basic knowledge of fractional calculus (FC) is introduced firstly. FC is a generalization of integration and differentiation operators, which is able to be represented as follows.

$${}_{t_0}D_t^{\alpha} = \begin{cases} \dfrac{d^{\alpha}}{dt^{\alpha}} & \mathrm{Re}(\alpha) > 0 \\ 1 & \mathrm{Re}(\alpha) = 0 \\ \displaystyle\int_{t_0}^{t} (d\tau)^{-\alpha} & \mathrm{Re}(\alpha) < 0 \end{cases} \tag{6}$$

where ${}_{t_0}D_t^{\alpha}$ denotes the FC; α is the fractional order; t_0 and t represent the upper and lower limits of the operation, respectively.

There are three mainstream methods to define the fractional operators [35]. The common one is the RL (Riemann Liouville) definition, which can be expressed as follows [36].

$${}_{t_0}D_t^{\alpha} f(t) = \frac{1}{\Gamma(n-\alpha)}\left(\frac{d}{dt}\right)^n \int_{t_0}^{t} \frac{f(\tau)}{(t-\tau)^{\alpha-n+1}} d\tau \tag{7}$$

where $(n-1 < \alpha < n, n \in N)$; $f(t)$ is the function; $\Gamma()$ is the well-known gamma function, which is described as follows.

$$\Gamma(z) = \lim_{n\to\infty} \frac{n! n^z}{z(z+1)\cdots(z+n)} \tag{8}$$

In this paper, the FOPID controller is used to control the road feeling, whose output voltage can be expressed as follows.

$$\begin{aligned} u(t) &= K_p e(t) + K_i D^{-\lambda} e(t) + K_d D^{u} e(t) \\ e(t) &= T(t) - T_s(t) \end{aligned} \tag{9}$$

where $K_p, K_i, K_d, \lambda, u$ are the proportional gain, integral gain, derivative gain, fractional order integrator, and fractional order differentiator, respectively.

The block diagram of road feeling control system using a FOPID controller is shown in Figure 3. The continuous transfer function of the FOPID controller is shown as follows.

$$G_C(s) = \frac{U(s)}{E(s)} = K_p + K_i s^{-\lambda} + K_d s^{u}, \quad (0 \le \lambda \le 2;\ 0 \le \mu \le 2) \tag{10}$$

Clearly, when $\lambda = 1, \mu = 1$, the FOPID controller becomes the conventional PID controller.

3.2. GA-Based Optimal Tuning of the FOPID Controller. GA is a search heuristic method that imitates the natural selection process, and it is an efficient technique to solve optimization problems [37, 38]. Hence, GA is used to tune five parameters of the FOPID controller in this paper, and its flow chart is shown in Figure 4.

Step 1. Once the approximate range and coding length of each parameter are determined, parameters are coded. In order to save the optimization time of GA, based on [11] and the optimization trials in MATLAB, the ranges of parameters are set as follows.

$$\begin{aligned} K_p &\in [0,1], \\ K_i &\in [0,20], \\ K_d &\in [0,1], \\ \lambda &\in [0,2], \\ \mu &\in [0,2] \end{aligned} \tag{11}$$

Compared with the real coding, the binary coding has simple coding and decoding operations, and it is easier to implement genetic operations. Therefore, the binary coding is selected to code five parameters of GA. The length of the binary string is calculated based on parameter range and optimization accuracy, which is shown below.

$$2^{i-1} \le (V_m - V_n) * 10^a \le 2^i - 1 \tag{12}$$

where i is the length of the binary string; V_m and V_n are the maximum and minimum values of the optimized parameters, respectively; a denotes the optimization accuracy of parameters.

Step 2. The initial population is randomly generated by the computer. For the binary coding, a random number of

Table 1: The actual parameters of the SBW system.

Symbol	Value	Unit
J_m	0.0068	kg.m^2
B_m	0.0165	N.m.s/rad
L	0.00033	H
R	0.183	Ω
K_e	0.07	V.s/rad
K_t	0.068	N.m/A
g_m	22	\

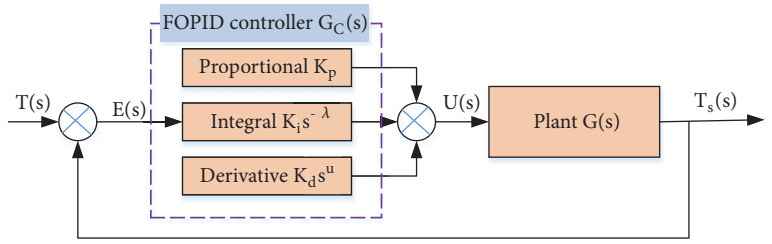

Figure 3: Block diagram of road feeling control system using a FOPID controller.

uniform distribution between 0~1 is created firstly, and then the random numbers between 0~0.5 are represented by 0; the random numbers between 0.5~1 are denoted by 1.

Step 3. The individual parameters of the population are decoded into corresponding values, and then the best individual is found through calculating the fitness function values. To define suitable fitness function, the objective function must be taken into account firstly. The common objective function of the FOPID controller is integral of squared error (ISE), integral of absolute value error (IAE), integral of time by absolute value error (ITAE), and integral of time by squared error (ITSE), which are defined as follows [9].

$$\begin{aligned} IAE &= \int_0^\infty |e|\, d_t, \\ ITAE &= \int_0^\infty t\,|e|\, d_t, \\ ISE &= \int_0^\infty e^2 d_t, \\ ITSE &= \int_0^\infty te^2 d_t \end{aligned} \tag{13}$$

The IAE criterion mentioned above is regarded as the objective function of the FOPID controller in this paper. Clearly, the smaller the value of IAE, the better the performance of the FOPID controller. GA is to search for individuals with maximum fitness function value. On that basis, the fitness function of GA is defined as follows.

$$f(x) = \frac{1}{IAE} = \frac{1}{\int_0^\infty |e|\, d_t}, \quad x = \left(K_p, K_i, K_d, \lambda, \mu\right) \tag{14}$$

Step 4. Check whether the genetic generation is reached. GA will output optimization results once the genetic generation is satisfied; otherwise, the fifth step will be executed.

Step 5. Genetic operators are implemented. The initial population can be used to obtain a new population through implementing reproduction, crossover, and mutation. The new generation is applied into Step 3, and then the fitness function value of new generation is obtained.

Step 6. Steps 3~5 are repeated until genetic generation is reached, and the best gene string is received. At last, five parameters of the FOPID controller can be obtained based on decoding operation.

All the parameters in the GA-based optimization process are defined as follows:

(i) Population size: 1000
(ii) Crossover probability: 0.5
(iii) Mutation probability: 0.02
(iv) Genetic algebra: 100

4. Fault Tolerant Module Based on Kalman Filter

By analyzing the overall road feeling control strategy mentioned above, it can be known that the torque sensor is of great significance as a feedback signal acquisition module. However, the faults of the torque sensor may appear in the long time process of the road feeling motor, which can cause a critical effect on the road feeling control. In this context, KF-based FTC method for the torque sensor is proposed in this paper.

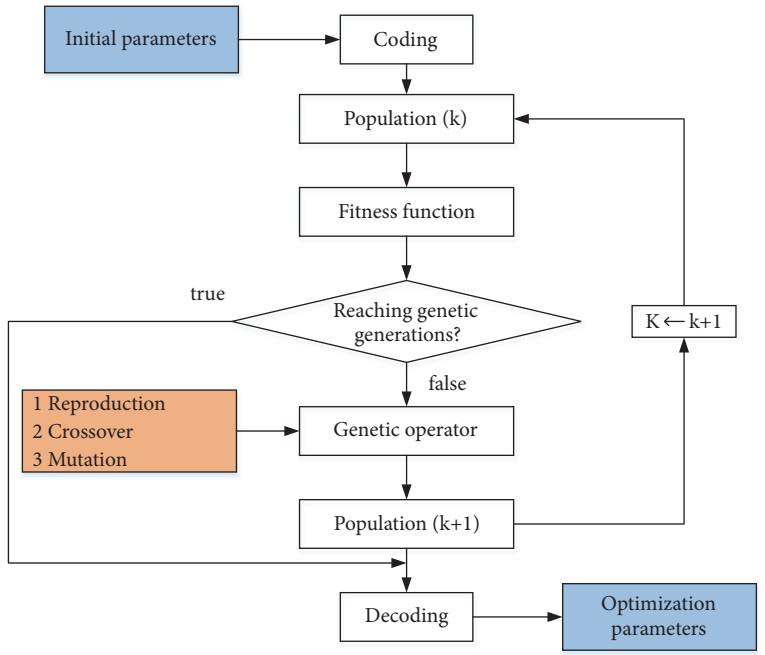

Figure 4: GA-based parameters optimization process.

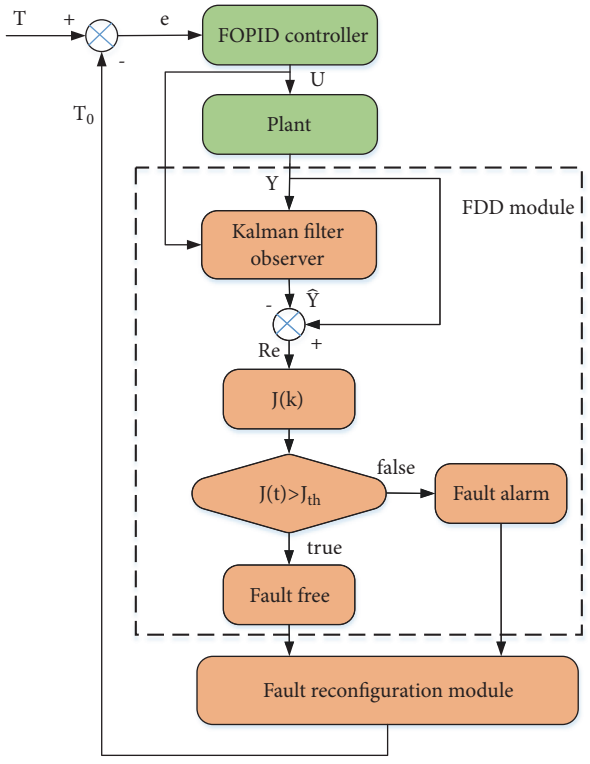

Figure 5: The fault tolerant control procedure.

The FTC procedure is shown in Figure 5. Firstly, the voltage output of the FOPID controller and the plant torque output signal are put into the KF observer. Secondly, the estimated torque value of the road feeling motor is obtained based on the KF observer. Thirdly, the residual signal Re is sent to a fault evaluation function $J(k)$. Fourthly, the torque sensor in fault condition depends on the comparison between the fault evaluation function and its threshold value. If the fault evaluation function is bigger than its threshold, the faults occur in the torque sensor; otherwise, the torque sensor works normally. Finally, the fault reconfiguration module outputs the torque signal T_0 to the FOPID controller. If the torque sensor faults occur, T_0 is the estimated torque $\hat{Y}$ of the KF observer; otherwise T_0 is the torque Y measured by the torque sensor. As mentioned above, the FTC method mainly consists of two parts: FDD module and fault reconfiguration module.

4.1. Fault Detection and Diagnosis Strategy. FDD module makes full use of KF to detect the torque sensor faults in this paper. KF is a kind of linear unscented filter, which obtains the optimal estimation of system state and system parameters under the condition of minimizing the error variance. KF can be implemented by recurrence formula in discrete domain, and the amount of computation and storage is greatly reduced, so it is easy to meet the real-time requirements. Owing to its advantages, KF is used to estimate the torque value of the road feeling motor.

4.1.1. Observer Design Based on Kalman Filter. For a dynamic system, it can be described by the following difference equation.

$$\begin{aligned} \dot{X}(t) &= A_1 X(t) + B_1 u(t) + w(t) \\ Y(t) &= C_1 X(t) + v(t) \end{aligned} \tag{15}$$

where X and Y denote the state matrix and the observation signal matrix of system, respectively; u represents the input signal matrix; A_1, B_1, and C_1 are the parameter matrixes of system; w and v denote the process noise and the measurement noise matrixes, and they need to meet the following relationships.

$$\begin{aligned} E[w(k)] &= 0, \\ E[v(k)] &= 0, \\ E\left[w(k)\, v^T(j)\right] &= 0 \\ E\left[w(k)\, w^T(j)\right] &= Q\delta_{kj}, \\ E\left[v(k)\, v^T(j)\right] &= R\delta_{kj} \end{aligned} \tag{16}$$

where $E[]$ denotes the mean value;

$$\delta_{kj} = \begin{cases} 1, & k = j \\ 0, & k \neq j. \end{cases} \tag{17}$$

For the control object's transfer function $G(s)$ in this paper, it can be translated into a state space, and the related parameters in (15) are shown as follows.

$$\begin{aligned} X &= \begin{bmatrix} x_1 & x_2 \end{bmatrix}^T, \\ Z &= T_s, \\ u &= U \\ A_1 &= \begin{bmatrix} -\dfrac{B_m R_a + K_t K_e}{J_m L_a} & \dfrac{B_m L_a + J_m R_a}{J_m L_a} \\ 1 & 0 \end{bmatrix} \\ B_1 &= \begin{bmatrix} 1 \\ 0 \end{bmatrix}, \\ C_1 &= \begin{bmatrix} \dfrac{g_m K_t B_m}{J_m L_a} & \dfrac{g_m K_t}{L_a} \end{bmatrix} \end{aligned} \tag{18}$$

The continuous model described in (15) is discretized as follows.

$$\begin{aligned} X(k+1) &= Ax(k) + Bu(k) + w(k) \\ Y(k+1) &= Cx(k+1) + v(k) \end{aligned} \tag{19}$$

where $A = e^{A_1 T}$, $B = (\int_0^T e^{A_1(T-\tau)} d\tau) B_1$, $C = C_1$; A denotes the system state transition matrix of the discrete description; B is the system input matrix of the discrete description; C is the system measurement matrix of the discrete description; T denotes the sample time.

The process of KF contains two steps: prediction module and correction module [39, 40].

(1) Prediction Module

$$\text{State prediction: } \widehat{X}\left(k+\frac{1}{k}\right) = A\widehat{X}\left(\frac{k}{k}\right) + Bu(k) \tag{20}$$

$$\begin{aligned} &\text{Error covariance matrix prediction: } \widehat{P}\left(k+\frac{1}{k}\right) \\ &= A\widehat{P}\left(\frac{k}{k}\right)A^T + Q \end{aligned} \tag{21}$$

(2) Correction Module

$$\text{Kalman gain matrix: } K(k+1) = \widehat{P}\left(k+\frac{1}{k}\right)C^T\left[C\widehat{P}\left(k+\frac{1}{k}\right)C^T + R\right] \tag{22}$$

$$\begin{aligned} &\text{State update: } \widehat{X}\left(k+\frac{1}{k}+1\right) = \widehat{X}\left(k+\frac{1}{k}\right) + K(k+1)\,\varepsilon(k+1) \\ &\varepsilon(k+1) = Y(k+1) - H\widehat{X}\left(k+\frac{1}{k}\right) \end{aligned} \tag{23}$$

$$\text{Error covariance matrix update: } \widehat{P}\left(k+\frac{1}{k}+1\right) = [I - K(k+1)H]\,\widehat{P}\left(k+\frac{1}{k}\right) \tag{24}$$

where $\widehat{X}(k+1/k)$ and $\widehat{P}(k+1/k)$ are the predicted state value and error covariance prediction value at the (k+1)th moment based on their values at the kth moment; $\widehat{X}(k/k)$ and $\widehat{P}(k/k)$ are the predicted state value and error covariance prediction value at the kth moment; $K(k+1)$ is the Kalman gain matrix at the (k+1)th moment; $Y(k+1)$ denotes the observation matrix at the (k+1)th moment; $\varepsilon(k+1)$ represents the innovation information of filtering at the (k+1)th moment.

4.1.2. Residual Generation and Evaluation. By means of (20)-(24), the torque value of the road feeling motor can be estimated effectively. The residual signal is the difference between the measured and estimated values described as follows [41].

$$r(k) = Y(k) - \widehat{Y}(k) \tag{25}$$

where $r(k)$ denotes the residual signal; $Y(k)$ represents the torque value measured by the torque sensor; $\widehat{Y}(k)$ is the torque value estimated by KF.

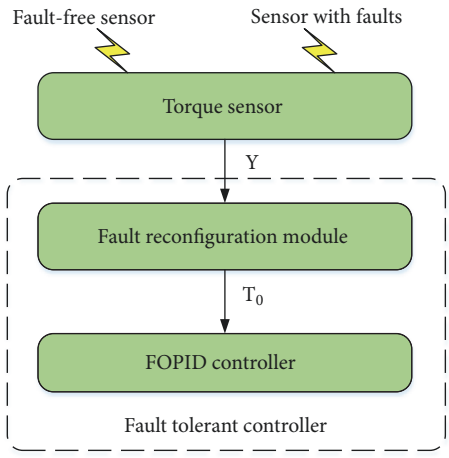

Figure 6: Control reconfiguration for sensor faults.

The fault evaluation function $J(k)$ can be defined as follows [42].

$$J(k) = |r(k)| \tag{26}$$

Suppose the threshold of the evaluation function is J_{th} which can be designed in experiments according to the experience of experts [42]. The torque sensor faults can be detected by the following rule.

$$\begin{aligned} J(k) < J_{th} &\Longrightarrow fault - free \\ J(k) \geq J_{th} &\Longrightarrow fault - alarm \end{aligned} \tag{27}$$

4.2. Fault Reconfiguration Strategy. If the torque sensor faults occur, the controller cannot control the road feeling of the SBW system correctly. To minimize the potential risks of sensor faults, the FTC strategy is needed to control the road feeling, which uses the fault reconfiguration module to output the torque to the proposed FOPID controller. The key point in the FTC strategy is to reconstruct the system torque output using the fault reconfiguration module. When the torque sensor is detected with faults based on the FDD module, the system torque output is the estimated value $\widehat{Y}(k)$ of KF. When the torque sensor is detected with no fault, the system torque output is the torque value $Y(k)$ measured by the torque sensor. Hence, the output T_0 of the fault reconfiguration module can be described as follows.

$$\begin{aligned} T_0 &= Y(k)\,(fault - free) \\ T_0 &= \widehat{Y}(k)\,(fault - alarm) \end{aligned} \tag{28}$$

Figure 6 shows the control reconfiguration strategy for the torque sensor faults. Based on the principle of the fault reconfiguration module, the FOPID can receive the valid torque value as a feedback signal whenever the sensor faults occur. In this way, the fault tolerant controller can ensure the normal road feeling control.

5. Simulation Results and Analyses

In this section, simulations based on MATLAB are carried out to validate the feasibility of the proposed FOPID controller and the FTC strategy.

5.1. Test of the FOPID Controller. In order to demonstrate the superiority of the FOPID controller, the conventional PID controller tuned by GA is also designed to compare the performance of the optimized FOPID controller. The code of GA is written in MATLAB to calculate the objective function mentioned in (14) for every set of parameters in the ranges described in (11). The optimization is executed for the FOPID controller and the conventional PID controller to find the optimal value $(K_p, K_i, K_d, \lambda, \mu)$ through minimizing IAE of the unit step responses of the ideal steering resistance torque. Table 2 shows the optimal parameters of the FOPID controller and the conventional PID controller using GA.

From Table 2, we can see that the optimized FOPID controller has better performance because the FOPID controller decreases by 68.83% compared with the conventional PID controller in terms of IAE. The FOPID controller possessing better control effect is accompanied with the fractional integration order and differentiation order optimized by GA. Meanwhile, it verifies that the fractional integration order and differentiation order of the FOPID controller provide indeed a larger tuning space for better control performance. Moreover, Table 2 indicates that GA can tune parameters of the FOPID and the conventional PID controllers well because two controllers' IAE are small significantly. Furthermore, the code of GA in MATLAB tuning parameters of the FOPID and PID controllers can be extended into other control applications conveniently.

The unit step responses of the ideal steering resistance torque $T(t) = 1\ (0 \leq t \leq 1)$ using the optimized FOPID controller and conventional PID controller are shown in Figure 7. It can be seen that the optimized PID controller has 0.026s rise time, 0.072s settling time, and 14.823N.m IAE. Also, with the optimized FOPID controller, the rise time is 0.01s, the settling time is 0.007s, and the IAE is 4.620N-m. The rise time, settling time, and IAE of the FOPID controller are significantly smaller than the PID controller. It is concluded that the optimized FOPID controller has a better performance than the optimized PID controller in terms of transient response.

Figure 8 illustrates the following curves of the optimized FOPID controller and conventional PID controller for the $T(t) = \sin(2 * pi * t)\ (0 \leq t \leq 1)$ sinusoidal signal. Figure 9 shows the resistance torque tracking error of the optimized FOPID and PID controllers. On the one hand, we can see that the optimized FOPID controller has smaller tracking error from Figures 8 and 9. On the other hand, compared with 30.320N.m IAE of the optimized PID controller, the optimized FOPID controller has 10.662N.m IAE. Therefore, we can safely come to the conclusion that the optimized FOPID controller has better resistance torque tracking performance than the optimized PID controller.

Table 2: The optimal parameters of the FOPID controller and the conventional PID controller using GA.

Controller	K_p	K_i	K_d	λ	μ	IAE	f(x)
PID	0.0684	20	0	1	1	14.823	0.067
FOPID	0.118	19.521	0.155	1.067	1.875	4.620	0.216

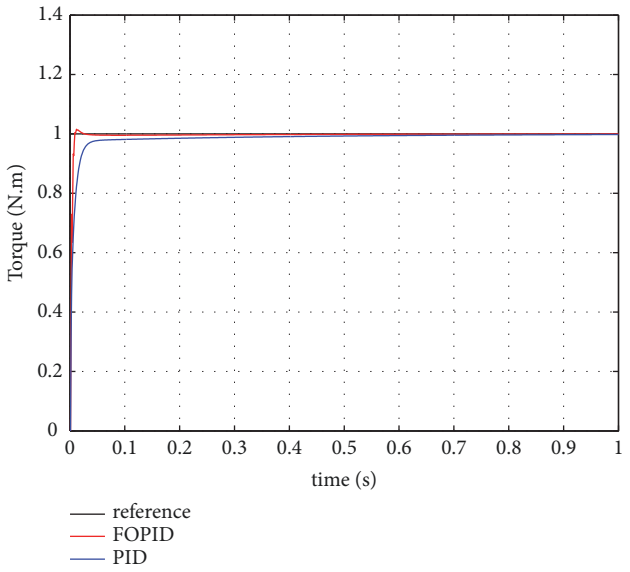

Figure 7: The unit step responses of the resistance torque using the optimized FOPID controller and conventional PID controller.

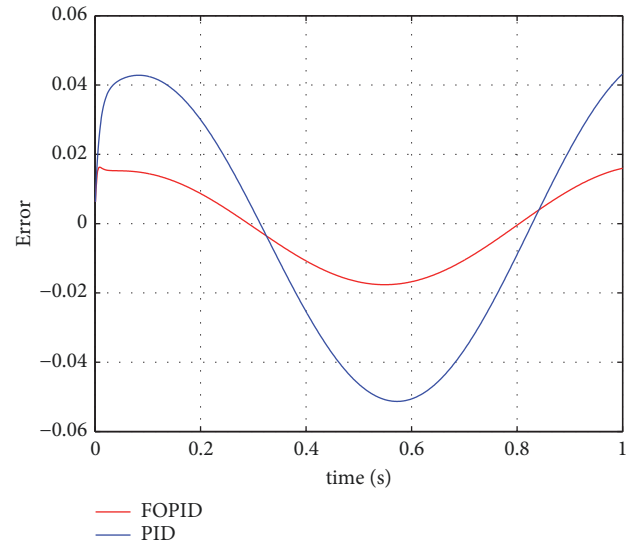

Figure 9: The resistance torque tracking error using the optimized FOPID and PID controllers.

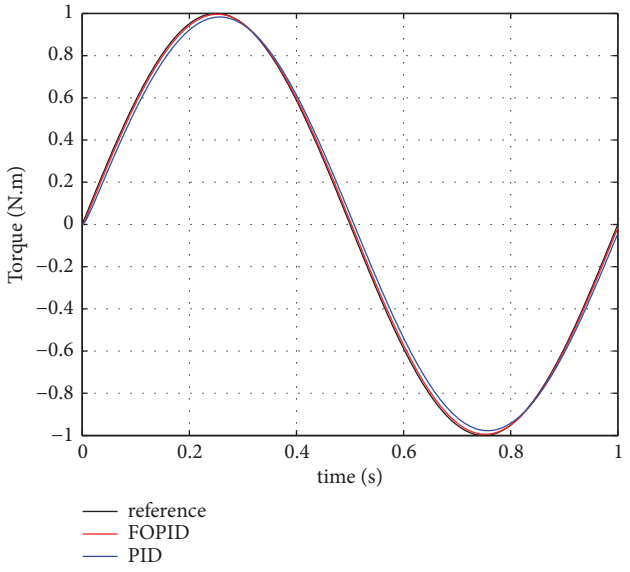

Figure 8: The sinusoidal following curve of the resistance torque based on the optimized FOPID and PID controllers.

5.2. Test of the Fault Tolerant Module. According to the above subsection, we can draw the conclusion that the FOPID controller has better transient response and tracking performance. The FOPID controller with the fault tolerant module is demonstrated in this subsection.

Firstly, the estimation accuracy of the KF observer is validated under the condition of the fault-free torque sensor. Figure 10(a) illustrates the KF-based estimation value and the measured value of the resistance torque. Figure 10(b) shows the estimation error of the resistance torque based on KF. From Figure 10, we can see that the KF observer has great estimation accuracy and it can be used to generate residual signal and detect sensor faults in the fault tolerant strategy.

Secondly, the fault tolerant schema is demonstrated based on simulations. In order to validate the comprehensive fault tolerant effect, three kinds of sensor faults (lock fault, constant gain fault, and constant deviation fault) are taken into account, which are shown as follows.

$$
\begin{aligned}
Y_1(t) &= a, \quad (|a| \geq J_{th},\ t \geq t_0) \\
Y_2(t) &= ky(t) + a, \quad (k \neq 0,\ k \neq 1,\ |a| \leq J_{th},\ t \geq t_0) \\
Y_3(t) &= y(t) + a, \quad (|a| \geq J_{th},\ t \geq t_0)
\end{aligned} \tag{29}
$$

where $Y_1(t)$, $Y_2(t)$, and $Y_3(t)$ denote the measured value by the torque sensor with lock fault, constant gain fault, and constant deviation fault, respectively; $y(t)$ represents the true value of the torque; k is the constant gain; a is the constant deviation; t_0 denotes the start time of sensor faults.

The specific sensor faults are simulated in the control system, which are shown below.

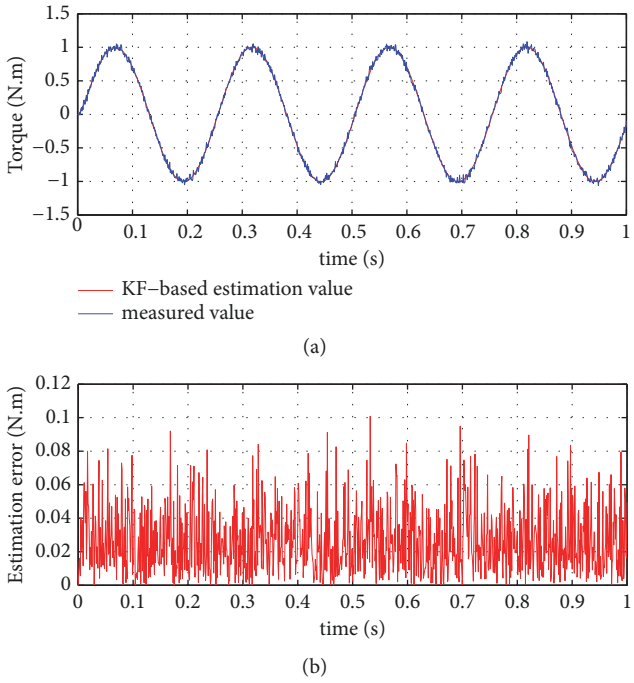

Figure 10: KF-based estimation performance of the resistance torque: (a) resistance torque; (b) estimation error.

$$Y_1(t) = 0.5, \quad (t \geq 0.5)$$

$$Y_2(t) = 3 * y(t) + 0.01, \quad (t \geq 0.4) \tag{30}$$

$$Y_3(t) = y(t) + 0.4, \quad (t \geq 0.6)$$

Figure 11 shows the fault detection result of the torque sensor with lock fault. The true value, KF-based estimation value, and value measured by the faulty sensor of the resistance torque are displayed in Figure 11(a). The fault evaluation function is shown in Figure 11(b). From Figure 11, we can clearly figure out that the sensor with the lock fault can be detected rapidly and effectively after it occurs. Furthermore, it can be seen that the estimation accuracy of KF is high and KF-based estimation value can be reconstructed as the torque feedback signal after the torque sensor's lock fault occurs.

Similarly, Figures 12 and 13 illustrate the fault detection results of the torque sensor with constant gain fault and constant deviation fault, respectively. From Figures 12 and 13, it can be seen that the faulty sensor can be detected once the sensor faults occur. KF-based estimation value also can be reconfigured as a substitute when the torque sensor fails.

Based on the simulation results mentioned above, we can draw the conclusions: (1) the FOPID controller tuned by GA has better control performance than the optimized PID controller in terms of transient response and tracking ability; (2) KF observer has great estimation accuracy, which can be used to generate residual signal and detect sensor faults; (3) the fault tolerant strategy can reconfigure the torque value rapidly and effectively when the torque sensor fails.

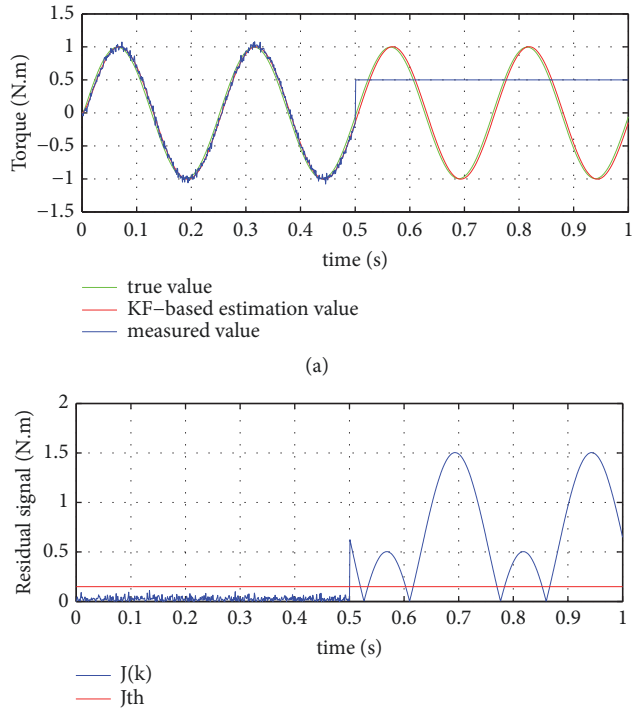

Figure 11: The fault detection result of the torque sensor with lock fault: (a) resistance torque; (b) residual signal.

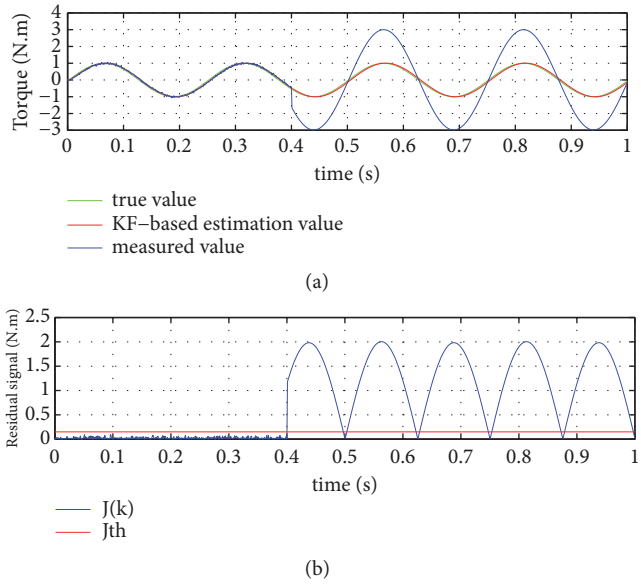

Figure 12: The fault detection result of the torque sensor with constant gain fault: (a) resistance torque; (b) residual signal.

6. Conclusions

In this paper, the FOPID controller with a fault tolerant module for the road feeling control of the SBW system is proposed. The FOPID controller is designed to control the steering resistance torque accurately and quickly. GA is applied to tune the FOPID's parameters including proportional constant,

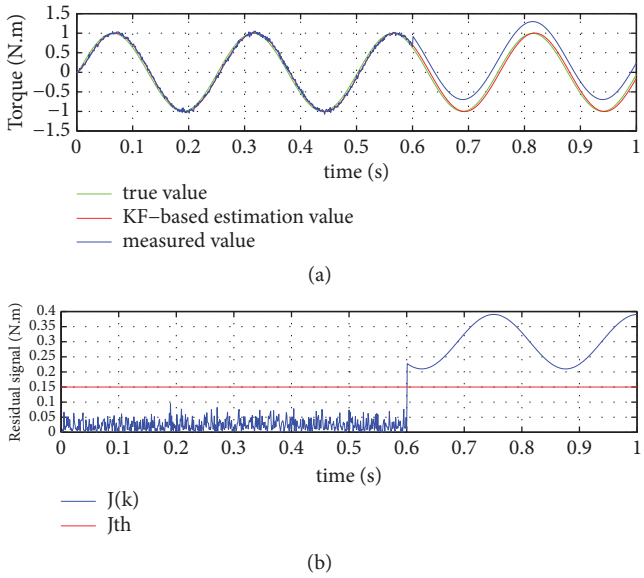

FIGURE 13: The fault detection result of the torque sensor with constant deviation fault: (a) resistance torque; (b) residual signal.

integral constant, derivative constant, integral order, and derivative order so as to achieve the best road feeling control performance that minimizes the IAE. In order to improve the reliability of the control system, a fault tolerant module aiming at the motor torque sensor is studied. In the FDD module, a residual signal is generated by KF, and a threshold of the fault evaluation function is used for judging sensor faults. For the fault reconfiguration module, the output torque of the control system can be reconstructed effectively when the torque sensor faults occur. Based on the fault tolerant strategy, the FOPID controller can receive the valid torque value as a feedback signal in spite of sensor faults. The results of the numerical simulations based on MATLAB demonstrate the effectiveness of the FOPID controller with a fault tolerant module. The optimized FOPID controller has better transient response and tracking performance than the traditional PID controller. The proposed FDD method can detect and diagnose the torque sensor faults (lock fault, constant gain fault, and constant deviation fault) effectively; what is more, the FTC strategy can identify and reconfigure faults within a reasonable time. Finally, the proposed FOPID controller with the FTC strategy can be extended into other industrial control applications.

Although the simulations based on MATLAB are carried out to demonstrate the feasibility of the proposed methods, the experiments conducted in practice would improve greatly the reliability and quality of this research. In the future, we will make joint efforts to complete the prototype vehicle, and then a large number of experiments with regard to the FOPID controller and the FTC strategy will be conducted and implemented on the prototype vehicle.

Data Availability

The data used to support the findings of this study are available from the corresponding author upon request.

Conflicts of Interest

The authors declare no conflicts of interest.

Acknowledgments

This research was funded by the National Key Research and Development Program of China under Grant No. 2016YFC0802904. The authors would like to acknowledge the Institute of Electrohydraulic Control Technology for Engineering Machinery in Jilin University and Xuzhou Construction Machinery Group Co., Ltd., which support this research.

References

[1] X. Wu, M. Zhang, M. Xu, and Y. Kakogawa, "Adaptive feedforward control of a steer-by-wire system by online parameter estimator," *International Journal of Automotive Technology*, vol. 19, no. 1, pp. 159–166, 2018.

[2] A. Balachandran and J. C. Gerdes, "Designing Steering Feel for Steer-by-Wire Vehicles Using Objective Measures," *IEEE/ASME Transactions on Mechatronics*, 2014.

[3] J. Iqbal, K. M. Zuhaib, C. Han, A. M. Khan, and M. A. Ali, "Adaptive global fast sliding mode control for steer-by-wire system road vehicles," *Applied Sciences (Switzerland)*, vol. 7, no. 7, 2017.

[4] M. Aly, M. Roman, M. Rabie, and S. Shaaban, "Observer-Based Optimal Position Control for Electrohydraulic Steer-by-Wire System Using Gray-Box System Identified Model," *Journal of Dynamic Systems, Measurement, and Control*, vol. 139, no. 12, 2017.

[5] H. Zhang and W. Zhao, "Two-way H∞ control method with a fault-tolerant module for steer-by-wire system," *Proceedings of the Institution of Mechanical Engineers, Part C: Journal of Mechanical Engineering Science*, vol. 232, no. 1, pp. 42–56, 2018.

[6] C. Kim, J. Jang, S. Yu, S. Lee, C. Han, and J. K. Hedrick, "Development of a control algorithm for a tie-rod-actuating steer-by-wire system," *Proceedings of the Institution of Mechanical Engineers, Part D: Journal of Automobile Engineering*, vol. 222, no. 9, pp. 1543–1557, 2008.

[7] S. M. H. Fahami, H. Zamzuri, S. A. Mazlan, and M. A. Zakaria, "Modeling and simulation of vehicle steer by wire system," in *Proceedings of the IEEE Symposium on Humanities, Science and Engineering Research (SHUSER '12)*, pp. 765–770, Kuala Lumpur, Malaysia, June 2012.

[8] H. Zang and S. Chen, "Electric power steering simulation analyze based on fuzzy PID current tracking control," *Journal of Computational Information Systems*, vol. 7, no. 1, pp. 119–126, 2011.

[9] X. Dong, D. Zhao, B. Yang, and C. Han, "Fractional-order control of active suspension actuator based on parallel adaptive clonal selection algorithm," *Journal of Mechanical Science and Technology*, vol. 30, no. 6, pp. 2769–2781, 2016.

[10] H. S. Li, Y. Luo, and Y. Q. Chen, "A fractional order proportional and derivative (FOPD) motion controller: tuning rule and experiments," *IEEE Transactions on Control Systems Technology*, vol. 18, no. 2, pp. 516–520, 2010.

[11] L. J. Bučanović, M. P. Lazarević, and S. N. Batalov, "The fractional PID controllers tuned by genetic algorithms for

expansion turbine in the cryogenic air separation process," *Hemijska Industrija*, vol. 68, no. 5, pp. 519–528, 2014.

[12] K. Vanchinathan and K. R. Valluvan, "A Metaheuristic Optimization Approach for Tuning of Fractional-Order PID Controller for Speed Control of Sensorless BLDC Motor," *Journal of Circuits, Systems and Computers*, vol. 27, no. 8, 2017.

[13] I. S. Jesus and R. S. Barbosa, "Design of Fuzzy Fractional PD + I Controllers Tuned by a Genetic Algorithm," *Mathematical Problems in Engineering*, vol. 2014, Article ID 676121, 14 pages, 2014.

[14] H. Anwaar, Y. Yixin, S. Ijaz, M. Ashraf, and W. Anwaar, "Fractional Order Based Computed Torque Control of 2-link Robotic Arm," *Advances in Science and Technology Research Journal*, vol. 12, no. 1, pp. 273–284, 2018.

[15] G. Zhang, X. Gong, and X. Chen, "PID control algorithm based on genetic algorithm and its application in electric cylinder control," *International Journal of Information Technology and Web Engineering*, vol. 12, no. 3, pp. 51–61, 2017.

[16] R. Pankaj, S. Vineet, and P. Om, "Determination of Stabilizing Parameter of Fractional Order PID Controller Using Genetic Algorithm," in *Proceedings of the Om P. Determination of Stabilizing Parameter of Fractional Order PID Controller Using Genetic Algorithm. International Journal of Computational Engineering Management*, vol. 15, pp. 24–32.

[17] I. S. Jesus and R. S. Barbosa, "Genetic optimization of fuzzy fractional PD+I controllers," *ISA Transactions®*, vol. 57, pp. 220–230, 2015.

[18] I. Chathoth, S. K. Ramdas, and S. T. Krishnan, "Fractional-order Proportional-integral-derivative-based Automatic Generation Control in Deregulated Power Systems," *Electric Power Components and Systems*, vol. 43, no. 17, pp. 1931–1945, 2015.

[19] I. Pan and S. Das, "Fractional-order load-frequency control of interconnected power systems using chaotic multi-objective optimization," *Applied Soft Computing*, vol. 29, pp. 328–344, 2015.

[20] S. Yim, "Fault-tolerant yaw moment control with steer - and brake-by-wire devices," *International Journal of Automotive Technology*, vol. 15, no. 3, pp. 463–468, 2014.

[21] J. S. Im, F. Ozaki, T. K. Yeu, and S. Kawaji, "Model-based fault detection and isolation in steer-by-wire vehicle using sliding mode observer," *Journal of Mechanical Science and Technology*, vol. 23, no. 8, pp. 1991–1999, 2009.

[22] J. Zarei and E. Shokri, "Robust sensor fault detection based on nonlinear unknown input observer," *Measurement*, vol. 48, no. 2, pp. 355–367, 2014.

[23] Y. Tian and F. Zhu, "Fault estimation and observer-based fault-tolerant controller in finite frequency domain," *Transactions of the Institute of Measurement and Control*, vol. 40, no. 5, pp. 1659–1668, 2018.

[24] S. K. Kommuri, S. B. Lee, and K. C. Veluvolu, "Robust sensors-fault-Tolerance with sliding mode estimation and control for PMSM drives," *IEEE/ASME Transactions on Mechatronics*, vol. 23, no. 1, pp. 17–28, 2018.

[25] M. Boukhari, A. Chaibet, M. Boukhnifer, and S. Glaser, "Proprioceptive Sensors' Fault Tolerant Control Strategy for an Autonomous Vehicle," *Sensors*, vol. 18, no. 6, article 1893, 2018.

[26] H. Zhang and J. Wang, "Active steering actuator fault detection for an automatically-steered electric ground vehicle," *IEEE Transactions on Vehicular Technology*, vol. 66, no. 5, pp. 3685–3702, 2017.

[27] A. Adnane, Z. Ahmed Foitih, M. A. Si Mohammed, and A. Bellar, "Real-time sensor fault detection and isolation for LEO satellite attitude estimation through magnetometer data," *Advances in Space Research*, vol. 61, no. 4, pp. 1143–1157, 2018.

[28] B. Pourbabaee, N. Meskin, and K. Khorasani, "Sensor fault detection, isolation, and identification using multiple-model-based hybrid Kalman filter for gas turbine engines," *IEEE Transactions on Control Systems Technology*, vol. 24, no. 4, pp. 1184–1200, 2015.

[29] S. Huang, K. K. Tan, and T. H. Lee, "Fault diagnosis and fault-tolerant control in linear drives using the Kalman filter," *IEEE Transactions on Industrial Electronics*, vol. 59, no. 11, pp. 4285–4292, 2012.

[30] G. Heredia and A. Ollero, "Detection of sensor faults in small helicopter UAVs using Observer/Kalman filter identification," *Mathematical Problems in Engineering*, vol. 2011, Article ID 174618, 20 pages, 2011.

[31] K. S. Xiahou and Q. H. Wu, "Fault-tolerant control of doubly-fed induction generators under voltage and current sensor faults," *International Journal of Electrical Power & Energy Systems*, vol. 98, pp. 48–61, 2018.

[32] Y. Liu, X. Zhang, and T. Zhang, "The Design and Semi-Physical Simulation Test of Fault-Tolerant Controller for Aero Engine," *International Journal of Turbo and Jet Engines*, vol. 34, no. 4, pp. 377–385, 2017.

[33] Q. Gong, *Study on Control Strategy and Road Feeling for Steering-By-Wire System*, Changan University, Xian, China, 2013.

[34] N. Kumar, B. Tyagi, and V. Kumar, "Application of fractional order PID controller for AGC under deregulated environment," *International Journal of Automation and Computing*, vol. 15, no. 1, pp. 84–93, 2018.

[35] G. Jumarie, "Modified Riemann-Liouville derivative and fractional Taylor series of nondifferentiable functions further results," *Computers & Mathematics with Applications*, vol. 51, no. 9-10, pp. 1367–1376, 2006.

[36] C. A. Monje, Y. Chen, B. M. Vinagre, D. Xue, and V. Feliu, *Fractional-Order Systems and Controls: Fundamentals and Applications*, Springer Science & Business Media, Berlin, Germany, 2010.

[37] M. Mitchell, *An Introduction to Genetic Algorithms*, MIT press, Cambridge, 1996.

[38] A. Muftah Almagrbi, T. Hatami, S. B. Glisic, and A. M. Orlović, "Determination of kinetic parameters for complex transesterification reaction by standard optimisation methods," *Hemijska Industrija*, vol. 68, no. 2, pp. 149–159, 2014.

[39] L. Li, G. Jia, X. Ran, J. Song, and K. Wu, "A variable structure extended Kalman filter for vehicle sideslip angle estimation on a low friction road," *Vehicle System Dynamics*, vol. 52, no. 2, pp. 280–308, 2014.

[40] R. E. Kalman, "A new approach to linear filtering and prediction problems," *Journal of Fluids Engineering*, vol. 82, no. 1, pp. 35–45, 1960.

[41] S. Cho, Z. Gao, and T. Moan, "Model-based fault detection, fault isolation and fault-tolerant control of a blade pitch system in floating wind turbines," *Journal of Renewable Energy*, vol. 120, pp. 306–321, 2018.

[42] L. Qin, X. He, R. Yan, and D. Zhou, "Active Fault-Tolerant Control for a Quadrotor with Sensor Faults," *Journal of Intelligent & Robotic Systems*, vol. 88, no. 2, pp. 1–19, 2017.